IEEE Access
Multidisciplinary | Rapid Review | Open Access Journal

Received 5 April 2024, accepted 25 April 2024, date of publication 29 April 2024, date of current version 6 May 2024.

Digital Object Identifier 10.1109/ACCESS.2024.3394737

RESEARCH ARTICLE

Model Predictive Control for Single-Stage Three-Phase Split Source Inverter With Enhanced Switched-Inductor Configuration

AHMED ABDELALEEM[1], AHMED ISMAIL M. ALI[1], (Member, IEEE), M. NASRALLAH[1], ESSAM E. M. MOHAMED[1], (Member, IEEE), HANY S. HUSSEIN[2], (Senior Member, IEEE), AND MOHAMED A. ISMEIL[1]

[1]Electrical Engineering Department, Faculty of Engineering, South Valley University, Qena 83523, Egypt
[2]Electrical Engineering Department, Faculty of Engineering, King Khalid University, Abha 61411, Saudi Arabia

Corresponding author: Ahmed Abdelaleem (ahmed.abdelaleem@eng.svu.edu.eg)

This work was supported by the Deanship of Scientific Research, King Khalid University, through the Large Group Research Project, under Grant RGP2/179/44.

ABSTRACT Power conversion systems need to meet various criteria, such as achieving optimal efficiency, minimizing costs and intricacy, and frequently enhancing boosting capabilities. This is commonly achieved through the utilization of a DC-DC boost converter (BC) at the front end preceding the inversion stage, resulting in a dual-stage structure. Conversely, single-stage power conversion systems, which integrate boosting within the inversion stage, provide potential benefits by simplifying system intricacy and reducing overall volume. Among various proposed alternatives, the split source inverter (SSI) has lately emerged as a viable replacement, presenting distinct features over the widely utilized Z-source inverter (ZSI). The boosting advantage of the SSI is comparable to that in the traditional BC, whereas it has been enhanced in numerous studies, particularly within impedance converters. This enhancement is essential for inverters with heightened voltage amplification is required, particularly when managing lower output voltage levels. To enhance this boosting function even more, a switched-inductor SSI (SL-SSI) has been created, substituting the conventional inductor with a switched-inductor within the SSI design. This paper investigates the performance of the SL-SSI using finite control set model predictive control (FCS-MPC) to validate the structure ability in providing high output-power quality. The suggested controller employs a discrete-time model to forecast input and output current behaviors for every switching state in the future via cost function reduction. The system's performance has been evaluated using MATLAB SIMULINK and validated with Opal-RT OP 4510. The system underwent exhaustive evaluation, analyzing step changes and varied load power conditions from 0.1 to 7 kW. The system results confirm a notable boosting capability, with observed increases up to tenfold supported by mathematical analysis for higher multiples. Furthermore, the controller exhibits rapid reference tracking, achieving settling times of around 10 milliseconds for input current and negligible for output current. Significantly, the system excels in generating high-quality output power, meeting low total harmonic distortion (THD) limits, which reach levels below 0.45% in the output current. Additionally, two comparative studies have been presented, assessing both the inverter structure and the control technique behavior.

INDEX TERMS Single-stage converter, split source inverter (SSI), switched-inductor (SL), model predictive control (MPC).

The associate editor coordinating the review of this manuscript and approving it for publication was Xiaodong Liang.

NOMENCLATURE

BC	Boost Converter.
RES	Renewable Energy Sources.

SSI	Split Source Inverter.
EV	Electric Vehicles.
ZSI	Z-source Inverter.
VSI	Voltage Source Inverter.
SL-SSI	Switched-inductor Split Source Inverter.
qZSI	quasi-Z-Source Inverter.
FCS-MPC	Finite Control Set Model Predictive Control.
SDSI	Split Delta Source Inverter.
THD	Total Harmonic Distortion.
SPWM	Sinusoidal Pulse Width Modulation.
CCM	Continuous Conduction Mode.
RMSVPWM	Regulated Modified Space Vector Pulse Width Modulation.

I. INTRODUCTION

Renewable energy sources are currently at the forefront of interest as substitutes for conventional energy sources, playing a crucial role in delivering sustainable and environmentally friendly power. Projections suggest that by 2040, approximately 35% of global energy production will be sourced from renewables [1]. The incorporation of renewable energy sources (RES) with electrical networks necessitates the development of interface devices, creating fertile ground for the advancement of power converter topologies. Beyond their significance in renewable energy, power converters are essential in diverse applications, including electric vehicles (EV) and various industrial contexts. Voltage source inverters (VSIs) stand out as the most widely utilized DC-AC power converters. VSIs possess inherent buck capabilities within the inversion stage, necessitating the incorporation of a DC-DC boosting stage to meet the applications requirements. This configuration is commonly referred to as a two-stage converter [2], [3], [4], [5]. In contrast, single-stage converters perform buck-boost operations, garnering increased concern owing to their compact volume, lower expense, lighter weight, and reduced intricacy [6], [7], [8], [9], [10]. Among the single-stage structures, the conventional Z-source inverter, illustrated in Fig. 1 [11], has emerged as a widely adopted design. Numerous derivative topologies have evolved from the Z-source inverter, including the quasi Z-Source Inverter (q-ZSI) [12], [13], [14], and the semi ZSI, which offers a cost-effective solution for photovoltaic systems [15]. The ZSI exhibits certain limitations, such as the requirement for additional switching states for boosting operations, discontinuous input current, and heightened inrush current. Addressing these challenges necessitates innovative solutions. A recent addition to the landscape of power converter configurations is the Split Source Inverter [16]. The nomenclature is derived from the division of the input voltage between the DC-link voltage on the capacitor and the boosted voltage on the inductor, as illustrated in Fig. 2.

As conventional configurations of three-phase Split Source Inverter (SSI) structures have been detailed in [17], [18], and [19], and their assorted advantages can be succinctly summarized as follows:

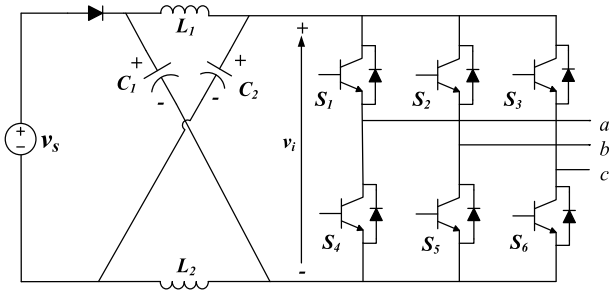

FIGURE 1. The conventional topology of Z-Source Inverter (ZSI).

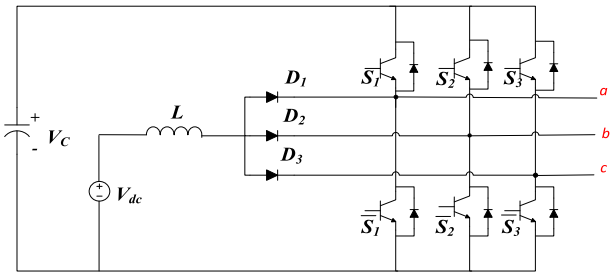

FIGURE 2. Split source inverter.

1. Reduced passive elements number compared to the ZSI.
2. Continuous input current operation.
3. Operation utilizing the same VSI eight states, derived from standard modulation schemes.
4. Stable inverter voltage with a low-frequency component.
5. Continuous DC-link voltage.
6. Mitigation of voltage stress on switches.

Numerous derived topologies have emerged with the aim of introducing new features or addressing specific challenges. One such modification involves the transition from a two-level operation in the Split Source Inverter (SSI) to a three-level operation. This transition brings added benefits to power conversion at high voltage levels, notably by minimizing voltage stresses on the switches and reducing the total harmonic distortion of the output voltage [20]. This advancement is achieved through the incorporation of a flying capacitor, as illustrated in Fig. 3a [21], [22]. The utilization of a flying capacitor enables a reduction in inductance requirements whereas maintaining an identical switching frequency. Nevertheless, this approach introduces a low-frequency component in the inverter voltage and input current due to the oscillation of flying capacitor voltages at lower frequencies. Another three-level architecture, employing a diode-clamped bridge as depicted in Fig. 3b, aims to alleviate current stresses on active switches [23]. Nevertheless, this configuration faces certain limitations concerning the low-frequency components in the inverter voltage and input current, as well as higher voltage stresses. Boosting capability enhancement and voltage

spike prevention in impedance-source inverters with leakage inductance and no absorption circuit were tackled by introducing a three-phase Split Delta Source Inverter (SDSI), as illustrated in Fig. 3c [24]. However, this solution is plagued by the occurrence of leakage current in the interconnected inductors. An alteration in a single-phase topology, featuring two common cathode diodes as illustrated in Fig. 3d, aimed to reduce parasitic inductance in commutation paths [25]. Unfortunately, this adjustment introduces a floating ground, thereby elevating the complexity of the gate driver design. The utilization of MOSFETs in lieu of BJTs and diodes served the purpose of diminishing switching and conduction losses while enabling bi-directional power flow [26]. In the quest for simplification, a streamlined single-phase topology was introduced (Fig. 3e) with the aim of reducing passive components and enhancing boosting gain [27]. Another different approach involved the use of reverse-blocking switches to replace the two clamping diodes in the conventional structure, thereby augmenting degrees of control freedom [28]. However, this adaptation also resulted in increased conduction losses. A recent topology called multi-input split source inverter (MISSI) is emerged to successfully deliver power from three separate sources to the grid [29]. Another configuration incorporates a voltage-boosting unit comprised of capacitors, inductors, and diodes, enhancing its capacity for boosting voltage [30]. TABLE 1 outlines the derived SSI structures found in the literature.

The topology and its associated structures underwent testing with various modulation schemes, with the conventional Sinusoidal pulse width modulation (SPWM) being employed in [31]. It is worth noting that the SPWM synthesizes variable duty ratio during inductor charging and discharging periods, which contributes to generating low-order harmonics and high total harmonic distortion (THD) due to the overmodulation. This prompts for the presentation of modified modulation schemes to address this challenge as hybrid quasi-sinusoidal and constant PWM [26] and regulated modified space vector PWM (RMSVPWM) [32].

Controlling converters is recognized as an effective approach to enhance their performance, with numerous studies and research articles being published annually on this subject. Recently, predictive control that has gained significant interest in power electronics applications [33], [34] as DC-DC converters [35], multilevel converters [36], electric motor drives [37], VSI [38] and impedance single-stage converters family [39], [40], [41]. Model predictive control (MPC), in its simplest form, is dependent on the mathematical model for the controlled variables to anticipate their future performance during the multiple switching states across a finite horizon time. A class inside MPC called Finite Control Set-MPC (FCS-MPC) implements the control instructions directly to the converter switches without the use of modulation techniques, however, it is limited by its variable switching frequency [42]. The control decision in FCS-MPC is chosen in accordance with the statement of the

TABLE 1. Highlights of the SSI derived structure.

Derived SSI structure	Main objective	Fig.3
[21]	minimizing voltage stresses on the switches and reducing the THD of the output voltage	a
[23]	aiming to alleviate current stresses on active switches	b
[24]	prevention of voltage spikes in similar impedance-source inverters with boosting capability enhancement	c
[25]	aiming to reduce parasitic inductance in commutation paths	d
[26]	diminishing switching and conduction losses while enabling bi-directional power flow	-
[27]	reducing passive components and enhancing boosting gain	e
[28]	augmenting degrees of control freedom	-
[29]	ability to inject power from different independent sources collectively	-
[30]	enhancing the capacity for boosting voltage	-

cost function. The converter switches in the following sample time should be optimized for the switching state with the minimal cost function. When this state is implemented, the minimum difference between the controlled variables and their desired values is applied. The weighting factor in the cost function equation is utilized to represent the significance of every variable in the control decision. Higher importance in the control decision is expressed by the larger weighting factor value. So, FCS-MPC has a lot of benefits over conventional PWM control techniques, which can be addressed as,

1. Controlling multiple control variables.
2. Implementation ease due to the discrete character of the switches.
3. Fast system response with enhanced performance.

However, it suffers from the long calculations required to obtain the optimal switching state that requires a long execution time inducing a considerable time delay in the control decision. This leads to a notable expansion of the ripple in the controlled current. Lately, FCS-MPC has been applied to control the SSI in [43], [44], [45], [46], and [47].

The SSI voltage boosting is insufficient for specific applications such as photovoltaic systems experiencing partial shading or wind farms operating during periods of low wind speed. Extensive literature enhancements have pushed the boosting gains of converters, particularly in single-stage configurations. Utilizing a switched-inductor (SL) offers a practical solution to amplify the boosting factor and enhances the inverter reliability, as evidenced in various studies such as [48], [49], and [50] with ZSI, [51] with qZSI, and [52] considering SSI in an open-loop approach. This paper introduces an innovative design, known as the three-phase switch-inductor split source inverter (SL-SSI), controlled by

FCS-MPC to power standalone loads. The paper examines the effectiveness of the proposed structure aiming to confirm its capability in delivering high-quality power output. In addition, the high voltage gain of the proposed topology forms a solution for the partial shading and low wind speed issues of photovoltaic wind farms. The MPC utilizes a discrete-time model of the SL-SSI to predict future behaviors of input and output currents for each switching state. The proposed controller is chosen to optimize topology performance, generate high-quality power outputs, and validate the topology's suitability for industrial applications.

Therefore, the noteworthy contributions of this manuscript can be listed as:

- An innovative design, referred as the three-phase switched-inductor split source inverter is presented to add a new value for the conventional SSI through the boosting capability.
- An appropriate FCS-MPC algorithm is used to regulate the SL-SSI structure.
- Two comparative analyses are presented, exhibiting the advantages of the proposed topology over recently published single-stage topologies, and the advantages of the proposed controller over the conventional ones.

This paper is structured as follows, the proposed inverter configuration and its mathematical model with controlled variables have been discussed in section II. The suggested control strategy has been discussed in section III, whereas the simulation and the real time validation have been described in sections IV and V, successively. In addition, two detailed comparisons have been presented in section VI. Ultimately, section VII summarizes the conclusion of the presented work.

II. CONVERTER MODELING BASED ON MPC

A. THREE-PHASE SL-SSI OPERATION

The traditional SSI contains the B6 bridge and the boosting circuit, which contains the inductor connected with the bridge via three diodes and the DC-link capacitor as depicted in Fig. 2. The proposed topology replaces the normal inductor with a switched-inductor configuration that comprises two inductors and three diodes as depicted in Fig. 4. One of the features of the proposed inverter structure is that it uses the same eight switches configuration of the VSI, as listed in TABLE 2. There are two main states among these states,

- Charging State: when one of the bottom switches is turned on, the inductors L_1 and L_2 are charging. The switched-inductor provides an extra feature during the charging state, wherein the two inductors are connected in parallel resulting in lowering the input inductance by forward biasing D_4 and D_6 and reverse biasing D_5 as depicted in Fig. 5a-g.
- Discharging state: only one condition allows the inductors and the source to discharge in the DC-link capacitor. This happens when all upper switches are active, hence the switched-inductor enables the inductors to be series by forward biasing D_5 and reverse biasing D_4 and D_6 as depicted in Fig. 5h.

TABLE 2. The switching states of switched-inductor SSI (SL-SSI).

States (S_1 S_2 S_3)	Inductor States		Capacitor States	Fig. 5
	L_1	L_2		
000	Charge	Charge	**Discharge**	(a)
100	Charge	Charge	**Discharge**	(b)
110	Charge	Charge	**Discharge**	(c)
010	Charge	Charge	**Discharge**	(d)
011	Charge	Charge	**Discharge**	(e)
001	Charge	Charge	**Discharge**	(f)
101	Charge	Charge	**Discharge**	(g)
111	**Discharge**	**Discharge**	Charge	(h)

The diodes configuration in the proposed inverter architecture exhibits required commutations during a single switching cycle, as seen in Fig. 5.

The behavior of the switched-inductor added the feature of high boosting gain to the conventional SSI. The equations below show the boosting gain of the conventional SSI and SL-SSI successively under the open loop condition [52].

$$B = \frac{1}{1-D} \tag{1}$$

$$B_{SL} = \frac{1+D}{1-D} \tag{2}$$

whereas B and B_{SL} are the boosting factors for SSI and SL-SSI successively, and D is the duty cycle. Fig. 6 illustrates the difference clearly.

B. MATHEMATICAL MODEL OF THE LOAD CURRENT

The switching states affect how the inverter output changes throughout the terminals of the RL load. To manage the complexity of three-phase systems, the variables are converted into two-phase (α, β) for analysis. The viable switching states of the SL-SSI are summarized in TABLE 3, whereas Fig. 7 displays the output voltage for each condition as space vectors.

The output voltage vector (V_x^k) is expressed as [38];

$$V_x^{(k)} = \frac{2}{3} V_C \cdot (S_1 + aS_2 + a^2 S_3) \tag{3}$$

whereas, $x = [0 : 7]$, V_C is the DC-link voltage over the capacitor, a is the unity vector and equals $\frac{-1}{2} + j\frac{\sqrt{3}}{2}$, and S_1, S_2, S_3 represent the switching states.

The output voltage can be concluded from the load parameters as follows:

$$V_x^{(k)} = R.i_o^k + L\frac{di_o^k}{dt} \tag{4}$$

whereas, R and L are the load resistance and inductance, and i_o^k is the output current at the present sampling time.

The forward Euler approximation takes the place of the load current derivative di/dt as follows [38]:

$$\frac{di_o^k}{dt} \approx \frac{i_o^k - i_o^{k-1}}{T_s} \tag{5}$$

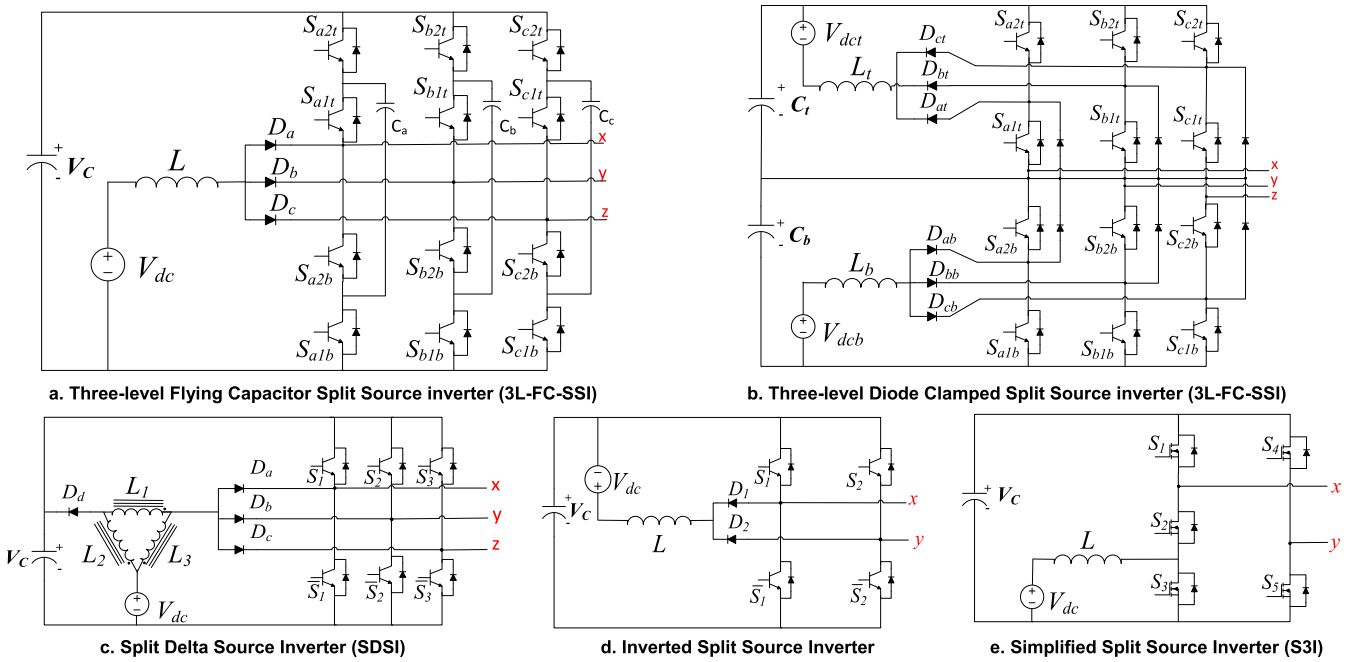

FIGURE 3. Different schemes derived from SSI.

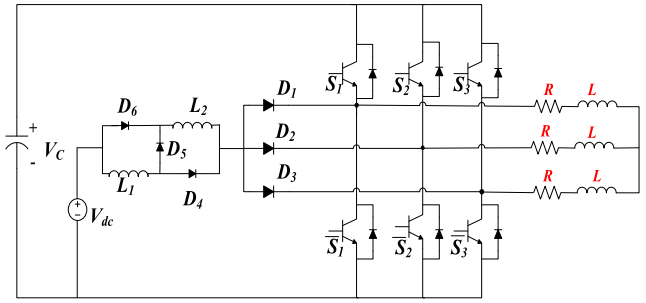

FIGURE 4. Switched-inductor Split Source Inverter (SL-SSI).

whereas, T_s is the sampling time and i_o^{k-1} is the output current at the previous sampling time.

In the light of equations (4) and (5), the output current i_o^k can be adjusted as

$$i_o^k = \frac{T_s \cdot V_x^k + L \cdot i_o^{k-1}}{L + R \cdot T_s} \tag{6}$$

By advancing the discrete-time one step in (6), it is possible to estimate the future load current by

$$i_o^{k+1} = \frac{T_s \cdot V_x^{k+1} + L \cdot i_o^k}{L + R \cdot T_s} \tag{7}$$

To establish the discrete model, it is essential to integrate the anticipated output current and its reference within the (α, β) coordinate system. The reference magnitude for the output current should be determined by relying on the desired output power. Subsequently, the cost function incorporates the absolute disparity between the setpoints and predicted values.

TABLE 3. Inverter output voltage in different switching states.

States (S_1, S_2, S_3)	Output Voltage $(V_\alpha + jV_\beta)$
000	$V_0 = 0$
100	$V_1 = \frac{2}{3}V_C$
110	$V_2 = \frac{1}{3}V_C + j\frac{\sqrt{3}}{3}V_C$
010	$V_3 = -\frac{1}{3}V_C + j\frac{\sqrt{3}}{3}V_C$
011	$V_4 = -\frac{2}{3}V_C$
001	$V_5 = -\frac{1}{3}V_C - j\frac{\sqrt{3}}{3}V_C$
101	$V_6 = \frac{1}{3}V_C - j.\frac{\sqrt{3}}{3}V_C$
111	$V_7 = 0$

C. MATHEMATICAL MODEL OF THE INPUT CURRENT

The control objectives require the mathematical model of the switched-inductor current in order to expect its future behavior at various switching states. The inductors in the switched-inductor have two main states, charging in parallel and discharging in series, as shown in Fig. 5.

- During the charging state:

Because $L_1 = L_2 = L$, the overall inductance of the switched-inductor is $L/2$

$$\frac{L}{2}\frac{di_l}{dt} = V_{dc} \tag{8}$$

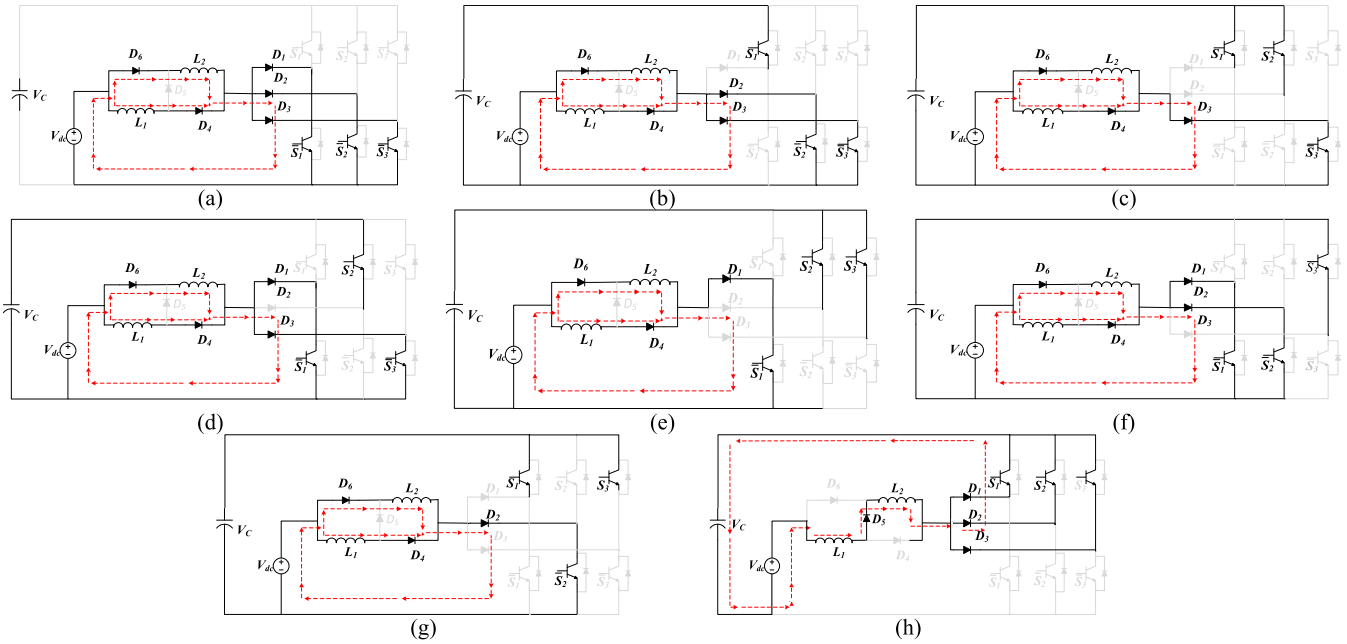

FIGURE 5. Switching states of three-phase SL-SSI without considering the load conditions.

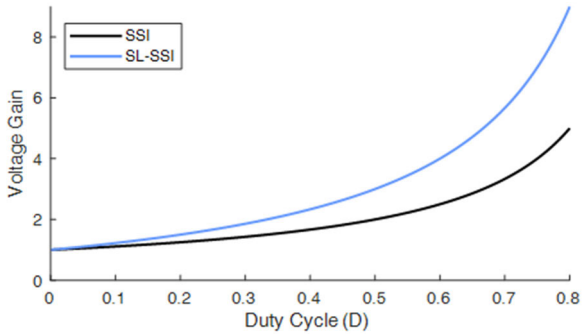

FIGURE 6. Voltage gains of the SSI and SL-SSI converters under duty cycle variation.

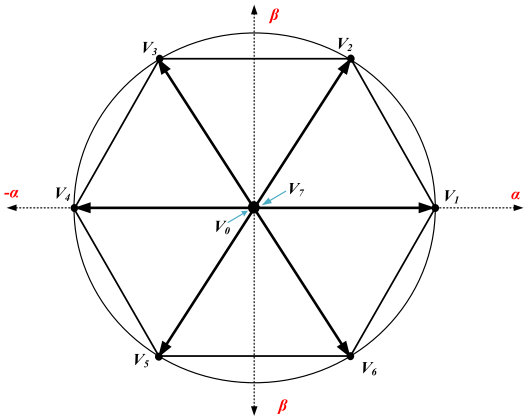

FIGURE 7. Space vectors of the output voltage in the complex plane (α,β).

whereas, i_l is input DC current and V_{dc} is the input DC source.

The future switched-inductor current under the discrete time model:

$$i_l^{k+1} = i_l^k + \frac{2T_s}{L} \cdot V_{dc}^k \tag{9}$$

whereas, i_l^{k+1} and i_l^k are the predicted and the current magnitudes of the switched-inductor current respectively, and V_{dc}^k is the present input voltage.

- During the discharging state:

The overall inductance of the switched-inductor is $2L$

$$2L\frac{di_l}{dt} = V_{dc} - V_C \tag{10}$$

whereas, V_C is the DC-link capacitor voltage.

Consequently, the future switched-inductor current under the discrete time model:

$$i_l^{k+1} = i_l^k + \frac{T_s}{2L} \cdot (V_{dc}^k - V_C^k) \tag{11}$$

whereas, V_C^k is the present DC-link voltage.

III. PROPOSED FCS-MPC ALGORITHM FOR SL-SSI

Fig. 8 depicts the proposed FCS-MPC with the SL-SSI approach. The proposed algorithm begins by monitoring the three-phase load currents, the capacitor voltage, and the input DC current at instant (k) with four current sensors and one voltage sensor.

The reference values for the three-phase current $i_{o\_ref}^{k+1}$ and the input DC current $I_{L\_ref}^{k+1}$ are separately determined using

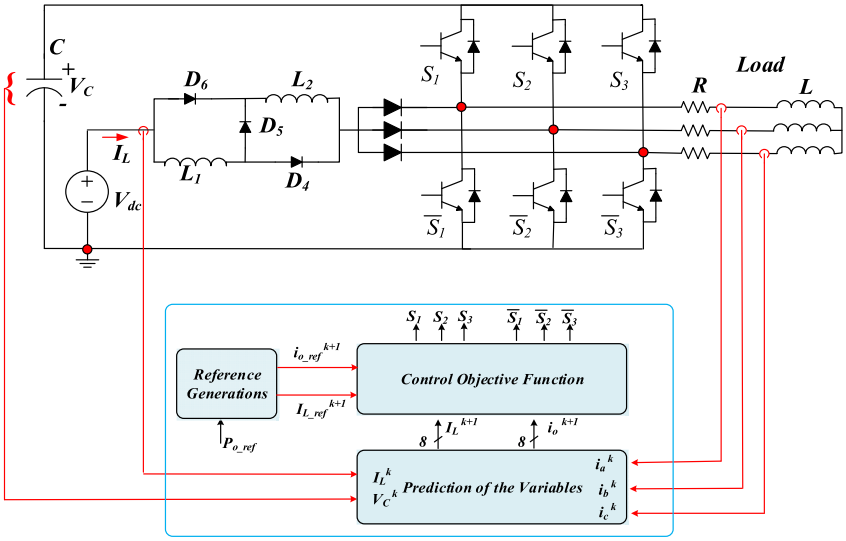

FIGURE 8. The proposed system block diagram considering the SL-SSI and its MPC-based control system.

the specified output power. The following step is to use (9) and (11) to determine the upcoming magnitude of the input DC current in both charging and discharging cases.

The cost function $g(i)$ is formulated by considering the discrepancies between the anticipated values and the reference values. Each error is given priority significance based on a its weight factor λ, The cost function can be defined as:

$$g(i) = \lambda_{io}(|i_{\alpha_{ref}}^{k+1} - i_{\alpha_o}^{k+1}| + |i_{\beta_{ref}}^{k+1} - i_{\beta_o}^{k+1}|) + \lambda_{IL}\left|I_{L_{ref}}^{k+1} - I_L^{k+1}\right| \quad (12)$$

whereas, $i_{\alpha_{ref}}^{k+1}$ is the real component of the reference output current, $i_{\alpha_o}^{k+1}$ is the real component of the predicted output current, $i_{\beta_{ref}}^{k+1}$ and $i_{\beta_o}^{k+1}$ represent the imaginary components of the reference and anticipated currents successively, $I_{L_{ref}}^{k+1}$ is the reference input DC current, I_L^{k+1} is the predicted input DC current, finally λ_{io} and λ_{IL} are the weighting factor of the output current and the input DC current respectively. The last step in the control technique is to calculate the cost function in each state and choose the optimum switching state to apply on the topology. The control steps of the proposed algorithm are organized in a flowchart as shown in Fig. 9.

IV. SIMULATION DISCUSSION

The proposed FCS-MPC technique-based SL-SSI was emulated using computer-aided MATLAB/SIMULINK software to assess the effectiveness of the proposed approach. The system contains a DC source with 50 *V*,a switched-inductor with two 3 mH inductors, and 470 μf DC-link capacitor as outlined in TABLE 4. To facilitate the inverter's functioning in Continuous Conduction Mode (CCM), to be applicable to diverse renewable energy applications such as PV systems and fuel cell applications, a high-value inductor in the *LC* network is chosen. The proposed system is connected to a standalone load, whereas the output current is regulated. Obviously, the SL-SSI supports the load with sinusoidal current waveforms following their reference waveforms. In addition, the output current waveforms have been step changed at instance 3*s*, as shown in Fig. 10. Concurrently, there is a step change in the load power, transitioning from 0.2 kW to 0.4 kW. This intentional step adjustment is implemented to affirm the capability of the proposed control method in accurately tracking the prescribed path of the regulated current. For a clearer understanding, a magnified view at the top of Fig. 10 has been incorporated. Fig. 11 depicts the voltage across the DC-link capacitor, demonstrating the step-adjusted DC voltage in sync with the variation in the load current. Whereas, Fig. 12 displays the input DC current that mirrors the current in the switched inductor, tracking its reference with swift dynamic responsiveness. This rapid attainment of steady-state affirms the efficacy of the proposed control strategy. Additionally, Fig. 13 and Fig. 14 present the waveforms of the load phase and line voltage, respectively, corresponding to the step-changed performance of the inverter load currents.

V. REAL TIME VALIDATION

To confirm the effectiveness of the proposed control strategy and validate its simulation outcomes, a real-time system of the SL-SSI has been carried out. For validation purposes, this real-world system employs the same parameters as those integrated into the simulation model. The system is energized by a 50V DC input source, with the DC-link capacitor holding a capacitance of 470μF, and the input inductor possessing an inductance of 3mH, as specified in TABLE 4. Also, the system parameters can be varied depending on the application, which decides the acceptable limit for input and output ripples, power quality, THD, and power factor.

TABLE 4. Design elements of SL-SSI system.

Parameter	Symbol	Value
DC Input Voltage	V_{dc}	50 V
Switched-inductor	$L_1 = L_2$	3 mH
DC-link Capacitor	C	470 μf
Output inductor	L	15 mH/phase
Output Resistant	R	10 Ω/phase
Sampling Time	T_s	10 μs

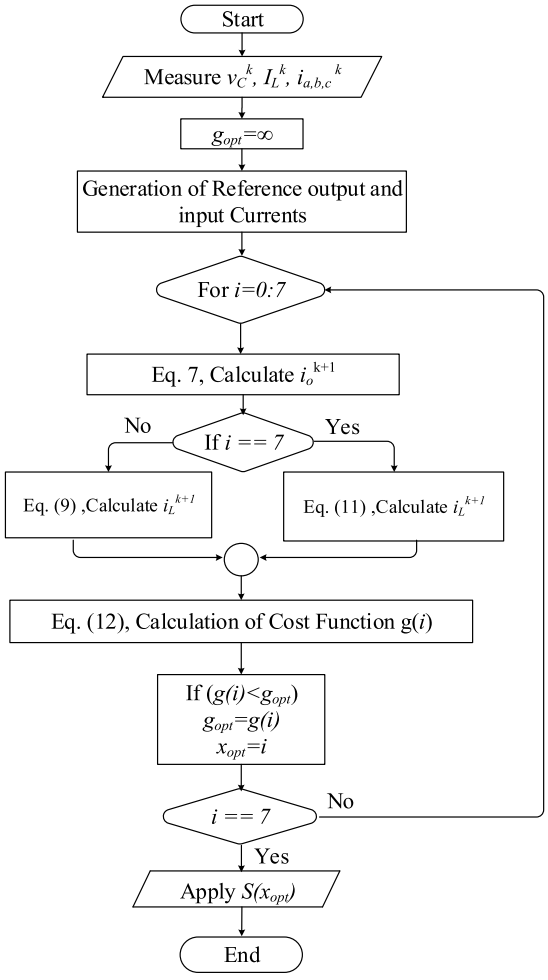

FIGURE 9. Flowchart of the MPC-based SL-SSI.

The MPC controller and the proposed converter are developed through M-files, MATLAB/Simulink, and RT-LAB block sets. The interfacing components connect the host PC to OP4510 and facilitate communications from OP4510 to the oscilloscope. The overarching block diagram illustrating the real-time operation is presented in Fig. 15. The entire system undergoes initial simulation in MATLAB/Simulink and subsequently, the execution takes place on the OP4510 workstation. By following the processing of data by OP4510, the outcomes are conveyed to the oscilloscope. The photographic representation of the system is depicted in Fig. 16.

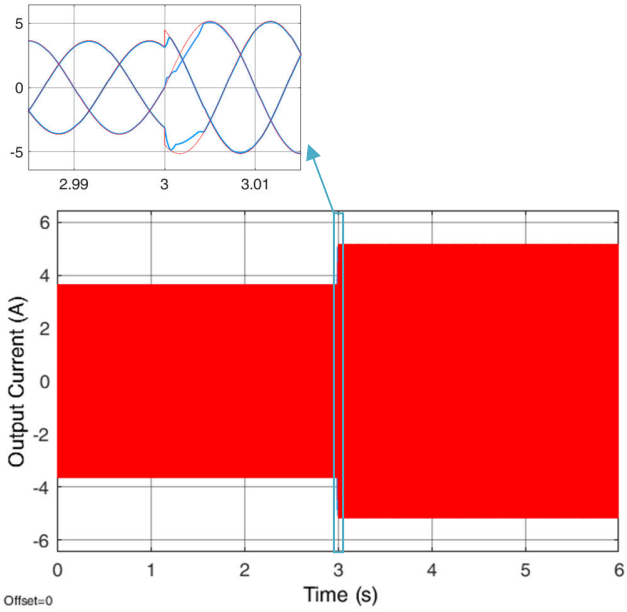

FIGURE 10. The SL-SSI three-phase output current and their reference ones considering power step-change between 0.2, and 0.4 kW.

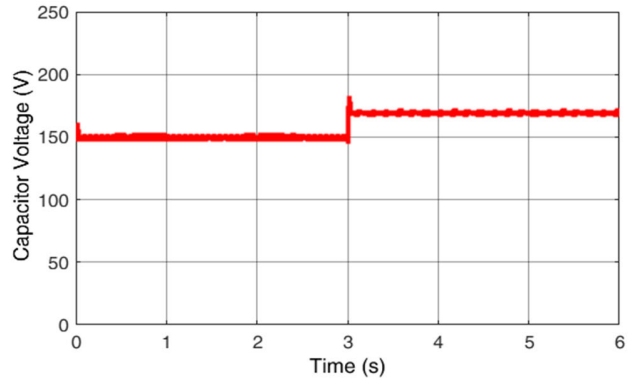

FIGURE 11. Capacitor voltage waveform of the SL-SSI considering power step-change between 0.2, and 0.4 kW.

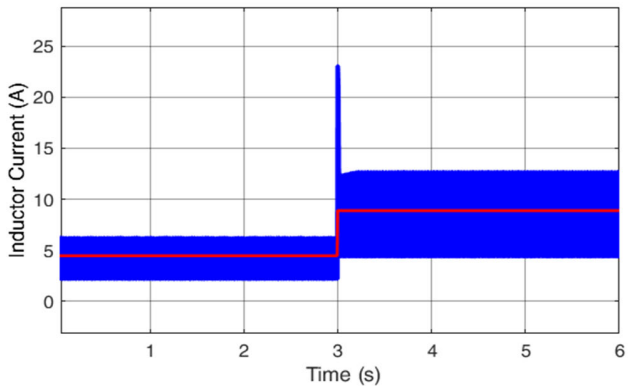

FIGURE 12. Input inductor reference and actual current waveforms considering power step-change between 0.2, and 0.4 kW.

The system is executed under various load power conditions to assess both the boosting capability of the proposed

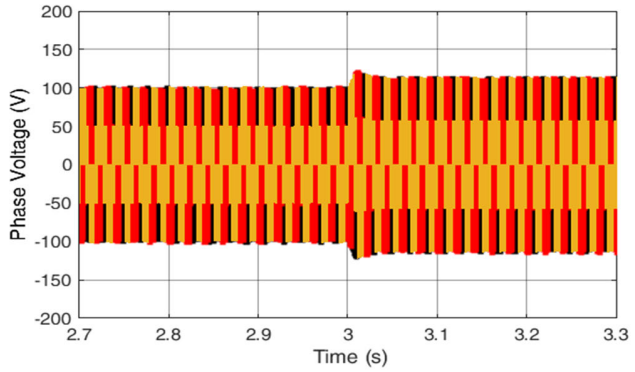

FIGURE 13. The MPC-based SL-SSI phase output voltage waveforms considering power step-change between 0.2, and 0.4 kW.

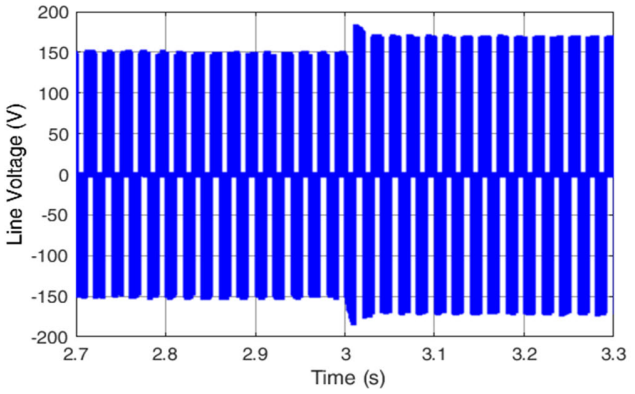

FIGURE 14. The MPC-based SL-SSI line output voltage considering power step-change between 0.2, and 0.4 kW.

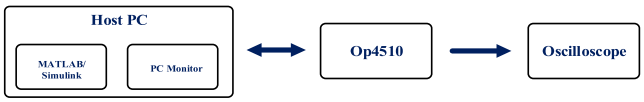

FIGURE 15. Real-time system block diagram.

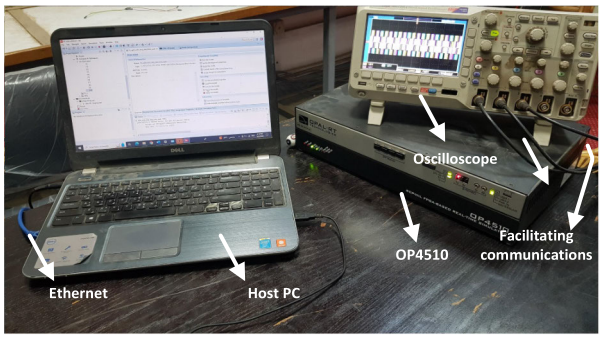

FIGURE 16. The real time system photograph.

structure and the effectiveness of the algorithm in adhering to the set references. The results in TABLE 5 display the THD and output currents for different load conditions. Evidently, the THD of the output current decreases initially, experiences a step rise at 3 kW, and then decreases again. This trend is

TABLE 5. The results of the proposed SL-SSI in different load conditions.

Output power	Output current	THD
0.1 kW	1.83 A	0.94%
0.3 kW	3.16 A	0.74%
0.5 kW	4.1 A	0.63%
0.7 kW	4.83 A	0.58%
0.9 kW	5.48 A	0.5%
1 kW	5.77 A	0.49%
1.5 kW	7.07 A	0.44%
2 kW	8.16 A	0.41%
3 kW	10 A	1.96%
4 kW	11.55 A	1.49%
5 kW	12.91 A	1.06%
6 kW	14.14 A	0.71%
7 kW	15.28 A	0.45%

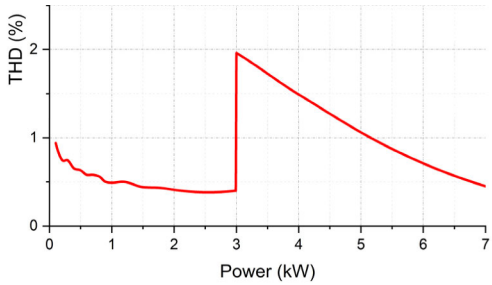

FIGURE 17. Load current THD variation under load change.

visually represented in Fig. 17, where THDs are compared against output power. The THD values distinctly indicate the topology's proficiency in generating high-quality power outputs. Additionally, the weighting factors in the cost function significantly influence the controller's behavior, delineating the shapes of the output and input currents. The algorithm employed prioritizes a higher output current weighting factor over the input current. Consequently, any alterations in the weighting factors will correspondingly alter the system's behavior under the same load conditions, which clarifies the rise in the THD value at 3 kW.

The system is tested with an output load of 0.2 kW, then stepped to 0.4 kW to assess the dynamic performance of the proposed control approach by stepping the peak value of output current from 3.65 A to 5.16 A, as illustrated in Fig. 18. Fig. 18 depicts one phase output current and its reference signal; the figure includes a zoomed-in section to clearly depict the dynamic response and how the real values closely follow the reference values. Fig. 19 shows these waveforms on the oscilloscope screen. The graph indicates that the steady state is reached within a short time of order microseconds which means that the settling time can be considered zero. This obviously shows the FCS-MPC capability of fast time response. Fig. 20 displays the three-phase output current, affirming the symmetry of the waveform and the adherence of each phase to its respective reference, whereas Fig. 21

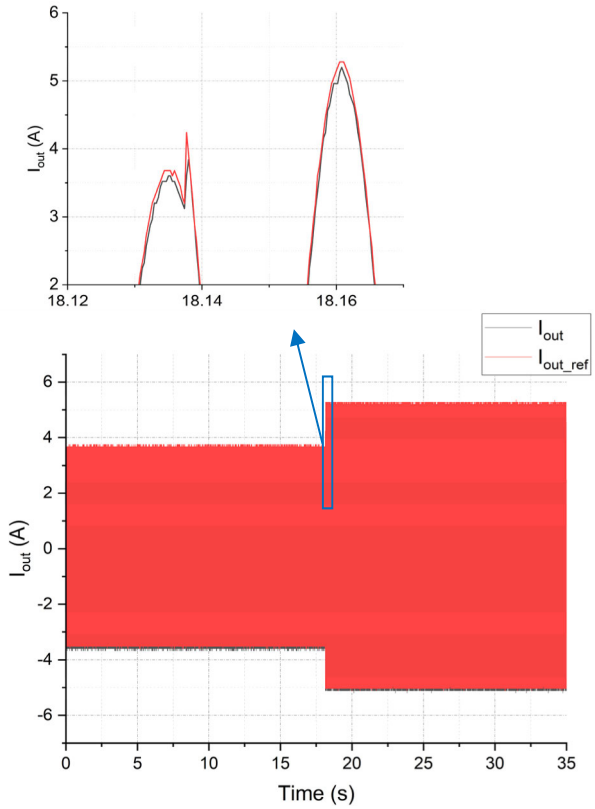

FIGURE 18. SL-SSI output current and its reference for output power step-changed from 0.2 to 0.4 *kW*.

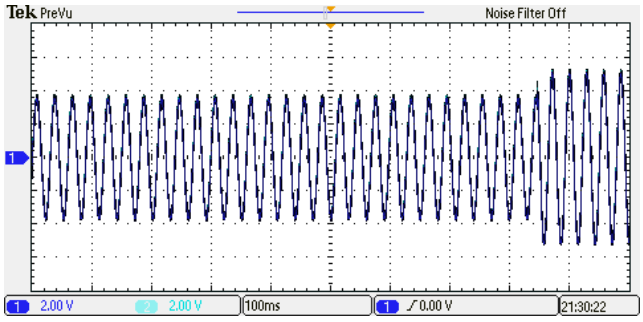

FIGURE 19. The oscilloscope screen of SL-SSI output current and its reference when for the output power step-changed from 0.2 to 0.4 *kW*.

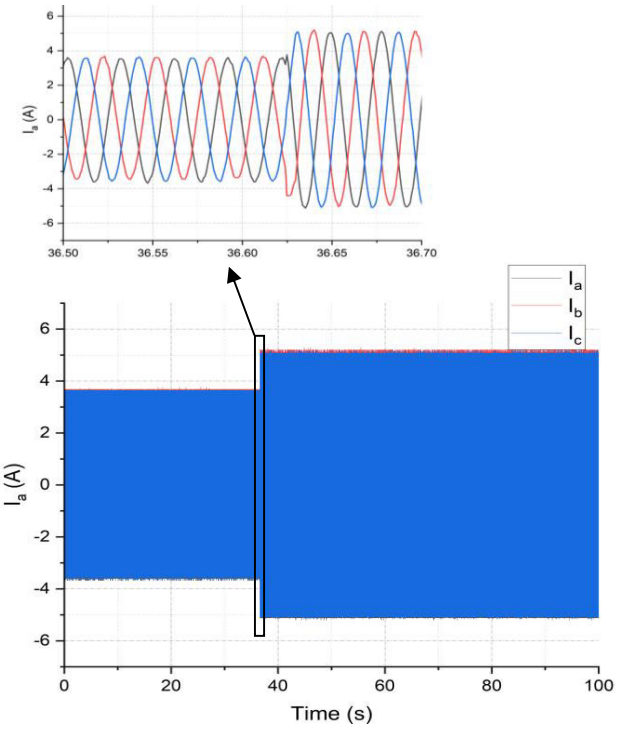

FIGURE 20. SL-SSI three-phase output current for output power step-changed from 0.2 to 0.4 *kW*.

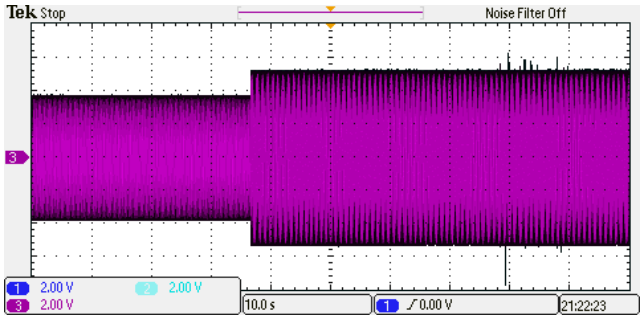

FIGURE 21. The oscilloscope screen of SL-SSI three-phase output current for the output power step-changed from 0.2 to 0.4 *kW*.

depicts it on the oscilloscope screen. Fig. 22 compares the input inductor current to its reference signal with around 10 ms settling time and proves MPC's strong dynamic responsiveness, whereas Fig. 23 presents them on the oscilloscope screen. Obviously, the input current overshoot is reduced in the real-time results due to the system parasitic inclusion compared to the simulation environments. In addition, Fig. 24 shows the DC-link voltage where its oscilloscope screen is portrayed in Fig. 25. Fig. 26 shows the three-phase output voltage on the oscilloscope display. Fig. 27 shows the line output voltage on the oscilloscope display.

The findings indicate that the suggested configuration exhibits a robust capability to elevate the input DC voltage to levels suitable for meeting the output specifications, and it is able to give outputs with low harmonic content. Also, the proposed algorithm works in different load cases, and the proposed control technique FCS-MPC has a very rapid response time, and the steady state is reached in a matter of microseconds.

VI. COMPARATIVE STUDY

The proposed structure is contrasted with the existing converter structures in [11], [12], [19], and [53] as shown in TABLE 6. The comparison is based on the family of the converter structure, number of switching, number of input diodes, number of input inductors, number of input capacitors, number of switching states, DC voltage gain and voltage stress. It is obvious that the proposed structure is more advantageous compared to the mentioned structures in the DC

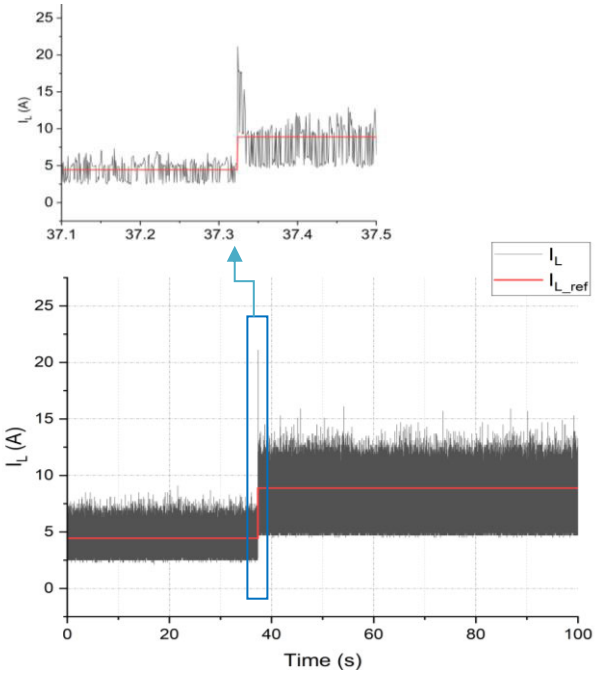

FIGURE 22. SL-SSI input inductor current for output power step-changed from 0.2 to 0.4 *kW*.

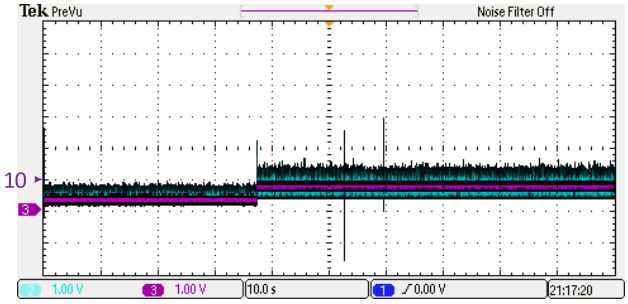

FIGURE 23. The oscilloscope screen of SL-SSI input inductor current for output power step-changed from 0.2 to 0.4 *kW*.

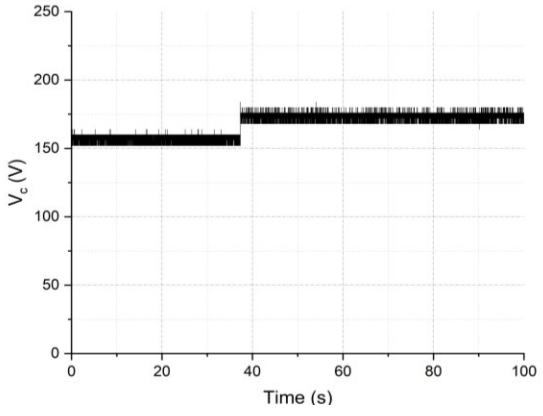

FIGURE 24. SL-SSI capacitor voltage for the output power step-changed from 0.2 to 0.4 kW.

voltage gain, which forms an important feature for renewable energy applications. Also, the proposed structure needs

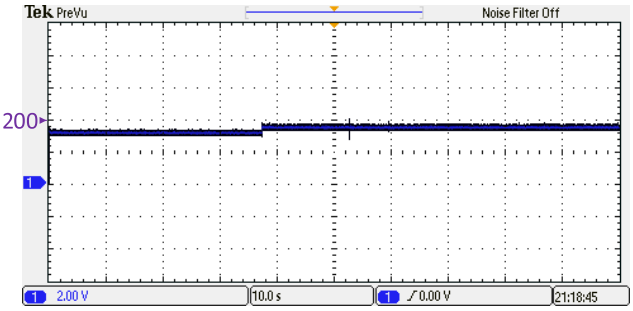

FIGURE 25. The oscilloscope screen of the SL-SSI capacitor voltage for the output power step-changed from 0.2 to 0.4 *kW*.

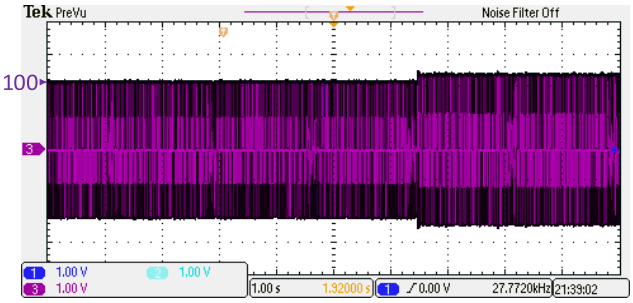

FIGURE 26. The oscilloscope screen of SL-SSI output three-phase voltage for output power step-changed from 0.2 to 0.4 *kW*.

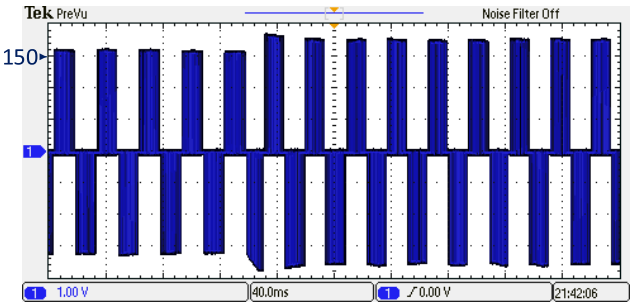

FIGURE 27. The oscilloscope screen of the SL-SSI output line voltage for the output power step-changed from 0.2 to 0.4 *kW*.

only eight switching states as the conventional SSI and VSI compared to nine in other single-stage structures, and it has a reduced number of passive components.

Moreover, the proposed control technique is contrasted with the existing control techniques in [54] and [55] as shown in TABLE 7. The comparison relies on the complexity in the implementation of the control technique, their dynamic response, modulation stage, control of multiple variables, THD of output current or voltage, switching frequency, and controller robustness. It is obvious that the proposed control technique is more advantageous than the other techniques in simplicity since no additional external hardware circuit is necessitated, fast tracking response, no modulation technique is required, the capability to control multivariable in a single cost function, and better output power quality.

TABLE 6. Comparison of other converter structures with the proposed structure.

Viewpoint	Buck-boost DC-DC+VSI [53]	ZSI [11]	q-ZSI [12]	SSI [19]	The proposed SL-SSI and [52]
Family	Two-stage	Single-stage	Single-stage	Single-stage	Single-stage
Nu. of switches	7	6	6	6	6
Nu. of input diodes	1	1	1	3	6
Nu. of input inductors	1	2	2	1	2
Nu. of input capacitors	1	2	2	1	1
Nu. of switching states	8	9	9	8	8
DC Voltage Gain	$\frac{D}{1-D}$	$\frac{1}{1-2D}$	$\frac{1}{1-2D}$	$\frac{1}{1-D}$	$\frac{1+D}{1-D}$
Voltage stress	$1+D$	$1+2D$	$1+2D$	$2+\sqrt{3}-\frac{1}{D}$	$\frac{1+3D}{1+D}$

TABLE 7. Comparison of two control approaches with the proposed approach for SSI family.

Viewpoint	PR&PI [55]	PI Decoupled [54]	The proposed FCS-MPC
Complexity in implementation	Complex, necessitate an additional hardare circuit	Complex, necessitate an additional hardare circuit	Straightforward, no external hardware circuit is necessitated.
Dynamic response	Slower in tracing the reference point	Slower in tracing the reference point	Swift in tracing the reference point
Modulating stage	Require a modulation technique	Require a modulation technique	Modulation technique is not required
Control of multiple variables	necessitate additional loops with intricacy in the design	necessitate additional loops with intricacy in the design	Incorporates this functionality within a single cost function
THD of output current/ voltage	2.25%	2.4%	Lower in all cases (0.44 - 1.96%)
Switching frequency	10 kHz	12 kHz	Variable
Robustness to variations in the input parameter	Tested for a step change in the input voltage from 100 V to 200 V	Tested for a step change in the input reference current from zero A to 10 A	Tested for a step change in the input current from 4.44 A to 8.88 A

VII. CONCLUSION

This study investigates the closed-loop control of the Switched-Inductor Split Source Inverter (SL-SSI) during standalone operation. By integrating the switched-inductor concept with the conventional Split Source Inverter (SSI), the converter's boosting gain range is expanded, theoretically reaching high levels and practically evaluated up to tenfold in the proposed system, which alleviates the problem of partial shading and low-speed weather for PV and wind farms, respectively. The introduced FCS-MPC algorithm facilitates unified control of the SSI's DC and AC sides through a single cost function, ensuring adaptability for diverse applications. Through MATLAB SIMULINK and validation with Opal RT OP4510, the MPC algorithm effectively guides output and input currents to closely track reference values, achieving low settling times around 10 ms in input current and nearly zero in output current, even during step changes. The control strategy demonstrates robust reference tracking capabilities, requiring no modulation techniques for implementation. Under varied load power conditions, THD values of the output current are below 0.45% limits which validate the proposed topology and control technique's capability to produce high-quality power output. Comparative analyses underscore the proposed topology's simplicity and boosting capability, alongside the control technique's effectiveness in precise tracking and straightforward implementation.

Additionally, the comparisons indicate that the structure may elevate conduction losses in certain components, and the variable switching frequency in the control approach could affect inverter efficiency. The SSI topology offers various aspects worthy of future exploration, such as adapting the power circuit to support multiple inputs and/or outputs. Additionally, addressing more control methods represents a crucial aspect for further investigation.

REFERENCES

[1] *World Energy Outlook*. Accessed: Jun. 2024. [Online]. Available: https://www.iea.org/reports/world-energy-outlook-2023

[2] L. Zhang, D. Xu, G. Shen, M. Chen, A. Ioinovici, and X. Wu, "A high step-up DC to DC converter under alternating phase shift control for fuel cell power system," *IEEE Trans. Power Electron.*, vol. 30, no. 3, pp. 1694–1703, Mar. 2015, doi: 10.1109/TPEL.2014.2320290.

[3] P. Cossutta, M. P. Aguirre, A. Cao, S. Raffo, and M. I. Valla, "Single-stage fuel cell to grid interface with multilevel current-source inverters," *IEEE Trans. Ind. Electron.*, vol. 62, no. 8, pp. 5256–5264, Aug. 2015, doi: 10.1109/TIE.2015.2434800.

[4] M. Forouzesh, Y. P. Siwakoti, S. A. Gorji, F. Blaabjerg, and B. Lehman, "Step-up DC–DC converters: A comprehensive review of voltage-boosting techniques, topologies, and applications," *IEEE Trans. Power Electron.*, vol. 32, no. 12, pp. 9143–9178, Dec. 2017.

[5] V. Samavatian and A. Radan, "A high efficiency input/output magnetically coupled interleaved buck–boost converter with low internal oscillation for fuel-cell applications: CCM steady-state analysis," *IEEE Trans. Ind. Electron.*, vol. 62, no. 9, pp. 5560–5568, Sep. 2015, doi: 10.1109/TIE.2015.2408560.

[6] O. Ellabban and H. Abu-Rub, "Z-source inverter: Topology improvements review," *IEEE Ind. Electron. Mag.*, vol. 10, no. 1, pp. 6–24, Mar. 2016.

[7] J. Cai and Q.-C. Zhong, "An asymmetrical GZ-source hybrid power converter with space vector pulse-width modulation," in *Proc. IEEE Energy Convers. Congr. Expo. (ECCE)*, Sep. 2014, pp. 344–349, doi: 10.1109/ECCE.2014.6953413.

[8] Y. P. Siwakoti, F. Z. Peng, F. Blaabjerg, P. C. Loh, and G. E. Town, "Impedance-source networks for electric power conversion part I: A topological review," *IEEE Trans. Power Electron.*, vol. 30, no. 2, pp. 699–716, Feb. 2015, doi: 10.1109/TPEL.2014.2313746.

[9] Y. P. Siwakoti, F. Z. Peng, F. Blaabjerg, P. C. Loh, G. E. Town, and S. Yang, "Impedance-source networks for electric power conversion Part II: Review of control and modulation techniques," *IEEE Trans. Power Electron.*, vol. 30, no. 4, pp. 1887–1906, Apr. 2015, doi: 10.1109/TPEL.2014.2329859.

[10] M. K. Nguyen, Y. C. Lim, and S. J. Park, "A comparison between single-phase quasi-ZSource and quasi-switched-boost inverters," *IEEE Trans. Ind. Electron.*, vol. 62, no. 10, pp. 6336–6344, 2015.

[11] F. Z. Peng, "Z-source inverter," in *Proc. Conf. Rec. IAS Annu. Meeting IEEE Ind. Appl. Soc.*, vol. 2, May 2002, pp. 775–781, doi: 10.1002/047134608x.w8348.

[12] Y. Li, J. Anderson, F. Z. Peng, and D. Liu, "Quasi-Z-Source inverter for photovoltaic power generation systems," in *Proc. 24th Annu. IEEE Appl. Power Electron. Conf. Expo.*, Feb. 2009, pp. 918–924, doi: 10.1109/APEC.2009.4802772.

[13] Y. Liu, H. Abu-Rub, and B. Ge, "Z-source/quasi-Z-source inverters: Derived networks, modulations, controls, and emerging applications to photovoltaic conversion," *IEEE Ind. Electron. Mag.*, vol. 8, no. 4, pp. 32–44, Dec. 2014, doi: 10.1109/MIE.2014.2307898.

[14] J. Anderson and F. Z. Peng, "A class of quasi-Z-source inverters," in *Proc. IEEE Ind. Appl. Soc. Annu. Meeting*, Oct. 2008, pp. 1–7, doi: 10.1109/08IAS.2008.301.

[15] T. Ahmed and S. Mekhilef, "Semi-Z-source inverter topology for grid-connected photovoltaic system," *IET Power Electron.*, vol. 8, no. 1, pp. 63–75, Jan. 2015, doi: 10.1049/iet-pel.2013.0486.

[16] H. Ribeiro, A. Pinto, and B. Borges, "Single-stage DC–AC converter for photovoltaic systems," in *Proc. IEEE Energy Convers. Congr. Expo.*, Sep. 2010, pp. 604–610, doi: 10.1109/ECCE.2010.5617957.

[17] M. A. Ismeil, A. Abdelaleem, A. Ismail M. Ali, M. Nasrallah, H. S. Hussein, and E. E. M. Mohamed, "A comparison analysis of a new switched-inductor and conventional split source inverter structures," *IEEE Access*, vol. 12, pp. 28013–28024, 2024, doi: 10.1109/ACCESS.2024.3366931.

[18] M. A. Ismeil, A. Abdelaleem, M. Nasrallah, and E. E. M. Mohamed, "Split source inverter: Topology and switching modulation improvements—A review," *E-Prime Adv. Electr. Eng., Electron. Energy*, vol. 5, Sep. 2023, Art. no. 100240, doi: 10.1016/j.prime.2023.100240.

[19] A. Abdelhakim, P. Mattavelli, and G. Spiazzi, "Three-phase split-source inverter (SSI): Analysis and modulation," *IEEE Trans. Power Electron.*, vol. 31, no. 11, pp. 7451–7461, Nov. 2016, doi: 10.1109/TPEL.2015.2513204.

[20] B. A. Welchko, M. B. de Rossiter Correa, and T. A. Lipo, "A three-level MOSFET inverter for low-power drives," *IEEE Trans. Ind. Electron.*, vol. 51, no. 3, pp. 669–674, Jun. 2004, doi: 10.1109/TIE.2004.825337.

[21] A. Abdelhakim, P. Mattavelli, and G. Spiazzi, "Three-phase three-level flying capacitors split-source inverters: Analysis and modulation," *IEEE Trans. Ind. Electron.*, vol. 64, no. 6, pp. 4571–4580, Jun. 2017, doi: 10.1109/TIE.2016.2645501.

[22] A. Abdelhakim, P. Mattavelli, and G. Spiazzi, "Three-level operation of the split-source inverter using the flying capacitors topology," in *Proc. IEEE 8th Int. Power Electron. Motion Control Conf.*, May 2016, pp. 223–228, doi: 10.1109/IPEMC.2016.7512289.

[23] A. Abdelhakim and P. Mattavelli, "Analysis of the three-level diode-clamped split-source inverter," in *Proc. 42nd Annu. Conf. IEEE Ind. Electron. Soc.*, Oct. 2016, pp. 3259–3264, doi: 10.1109/IECON.2016.7793581.

[24] X. Fang, W. Zhang, X. Kan, and Q. Wang, "Three-phase split delta-source inverter: Operating principles and modulation," in *Proc. IEEE 3rd Student Conf. Electr. Mach. Syst. (SCEMS)*, Dec. 2020, pp. 775–780, doi: 10.1109/SCEMS48876.2020.9352323.

[25] A. Abdelhakim, P. Mattavelli, P. Davari, and F. Blaabjerg, "Performance evaluation of the single-phase split-source inverter using an alternative DC–AC configuration," *IEEE Trans. Ind. Electron.*, vol. 65, no. 1, pp. 363–373, Jan. 2018, doi: 10.1109/TIE.2017.2714122.

[26] S. S. Lee and Y. E. Heng, "Improved single-phase split-source inverter with hybrid quasi-sinusoidal and constant PWM," *IEEE Trans. Ind. Electron.*, vol. 64, no. 3, pp. 2024–2031, Mar. 2017, doi: 10.1109/TIE.2016.2624724.

[27] S. S. Lee, A. S. T. Tan, D. Ishak, and R. Mohd-Mokhtar, "Single-phase simplified split-source inverter (S3I) for boost DC–AC power conversion," *IEEE Trans. Ind. Electron.*, vol. 66, no. 10, pp. 7643–7652, Oct. 2019, doi: 10.1109/TIE.2018.2886801.

[28] C. Yin, W. Ding, L. Ming, and P. C. Loh, "Single-stage active split-source inverter with high DC-link voltage utilization," *IEEE Trans. Power Electron.*, vol. 36, no. 6, pp. 6699–6711, Jun. 2021, doi: 10.1109/TPEL.2020.3038688.

[29] G. M. Cocco, F. Ecke Bisogno, R. F. de Camargo, and F. B. Grigoletto, "Multi-input split-source inverter (MISSI)," in *Proc. 14th Seminar Power Electron. Control (SEPOC)*, Nov. 2022, pp. 1–6, doi: 10.1109/SEPOC54972.2022.9976412.

[30] M. Wageh Lotfy, S. M. Dabour, R. Mahmoud Mostafa, D. J. Almakhles, and M. F. Elmorshedy, "Modeling and control of a voltage-lift cell split-source inverter with MPPT for photovoltaic systems," *IEEE Access*, vol. 11, pp. 54699–54712, 2023, doi: 10.1109/ACCESS.2023.3280602.

[31] A. Nahavandi, M. Roostaee, and M. R. Azizi, "Single stage DC–AC boost converter," in *Proc. 7th Power Electron. Drive Syst. Technol. Conf. (PEDSTC)*, Feb. 2016, pp. 362–366, doi: 10.1109/PEDSTC.2016.7556888.

[32] M. F. Elmorshedy, A. A. Abd-Elaziz, S. M. Dabour, M. E. Farrag, F. F. M. El-Sousy, W. Xu, and E. M. Rashad, "Performance investigation and control design of SSI grid-connected system for PV applications with maximum power extraction," *Alexandria Eng. J.*, vol. 78, pp. 354–366, Sep. 2023.

[33] S. Vazquez, J. I. Leon, L. G. Franquelo, J. Rodriguez, H. A. Young, A. Marquez, and P. Zanchetta, "Model predictive control: A review of its applications in power electronics," *IEEE Ind. Electron. Mag.*, vol. 8, no. 1, pp. 16–31, Mar. 2014, doi: 10.1109/MIE.2013.2290138.

[34] P. Cortes, M. P. Kazmierkowski, R. M. Kennel, D. E. Quevedo, and J. Rodriguez, "Predictive control in power electronics and drives," *IEEE Trans. Ind. Electron.*, vol. 55, no. 12, pp. 4312–4324, Dec. 2008, doi: 10.1109/TIE.2008.2007480.

[35] P. Karamanakos, T. Geyer, and S. Manias, "Direct voltage control of DC–DC boost converters using enumeration-based model predictive control," *IEEE Trans. Power Electron.*, vol. 29, no. 2, pp. 968–978, Feb. 2014, doi: 10.1109/TPEL.2013.2256370.

[36] J. Böcker, B. Freudenberg, A. The, and S. Dieckerhoff, "Experimental comparison of model predictive control and cascaded control of the modular multilevel converter," *IEEE Trans. Power Electron.*, vol. 30, no. 1, pp. 422–430, Jan. 2015, doi: 10.1109/TPEL.2014.2309438.

[37] S. Bolognani, S. Bolognani, L. Peretti, and M. Zigliotto, "Design and implementation of model predictive control for electrical motor drives," *IEEE Trans. Ind. Electron.*, vol. 56, no. 6, pp. 1925–1936, Jun. 2009, doi: 10.1109/TIE.2008.2007547.

[38] J. Rodriguez, J. Pontt, C. Silva, P. Cortes, U. Amman, and S. Rees, "Predictive current control of a voltage source inverter," in *Proc. IEEE 35th Annu. Power Electron. Spec. Conf.*, Dec. 2004, pp. 2192–2196, doi: 10.1109/PESC.2004.1355460.

[39] A. Bakeer, M. A. Ismeil, and M. Orabi, "A powerful finite control set-model predictive control algorithm for quasi Z-source inverter," *IEEE Trans. Ind. Informat.*, vol. 12, no. 4, pp. 1371–1379, Aug. 2016, doi: 10.1109/TII.2016.2569527.

[40] M. Mosa, O. Ellabban, A. Kouzou, H. Abu-Rub, and J. Rodríguez, "Model predictive control applied for quasi-Z-source inverter," in *Proc. 28th Annu. IEEE Appl. Power Electron. Conf. Expo. (APEC)*, Mar. 2013, pp. 165–169, doi: 10.1109/APEC.2013.6520202.

[41] S. Sajadian and R. Ahmadi, "Model predictive control of dual-mode operations Z-source inverter: Islanded and grid-connected," *IEEE Trans. Power Electron.*, vol. 33, no. 5, pp. 4488–4497, May 2018, doi: 10.1109/TPEL.2017.2723358.

[42] J. Rodriguez, M. P. Kazmierkowski, J. R. Espinoza, P. Zanchetta, H. Abu-Rub, H. A. Young, and C. A. Rojas, "State of the art of finite control set model predictive control in power electronics," *IEEE Trans. Ind. Informat.*, vol. 9, no. 2, pp. 1003–1016, May 2013, doi: 10.1109/TII.2012.2221469.

[43] M. A. Ismeil, "High dynamic performance for split-source inverter based on finite control set model predictive control," in *Proc. 21st Int. Middle East Power Syst. Conf. (MEPCON)*, Dec. 2019, pp. 8–13.

[44] Y. Elthokaby, I. Abdelsalam, N. Abdel-Rahim, and I. Mohamed, "Simplified three-phase split-source inverter for PV system application controlled via model-predictive control," *Int. J. Circuit Theory Appl.*, vol. 52, no. 5, pp. 2266–2289, May 2024.

[45] N. Güler, "Multi-objective cost function based finite control set-sliding mode control strategy for single-phase split source inverters," *Control Eng. Pract.*, vol. 122, May 2022, Art. no. 105114, doi: 10.1016/j.conengprac.2022.105114.

[46] N. Guler and H. Komurcugil, "Energy function based finite control set predictive control strategy for single-phase split source inverters," *IEEE Trans. Ind. Electron.*, vol. 69, no. 6, pp. 5669–5679, Jun. 2022, doi: 10.1109/TIE.2021.3090715.

[47] Y. Elthokaby, I. Abdelsalam, N. Abdel-Rahim, and I. Mohamed, "Standalone PV-based single-phase split-source inverter using model-predictive control," *Alexandria Eng. J.*, vol. 62, pp. 357–367, Jan. 2023.

[48] M. Zhu, K. Yu, and F. L. Luo, "Switched inductor Z-source inverter," *IEEE Trans. Power Electron.*, vol. 25, no. 8, pp. 2150–2158, Aug. 2010, doi: 10.1109/TPEL.2010.2046676.

[49] M. Ismeil, R. Kennel, and H. Abu-Rub, "Modeling and experimental study of three-phase improved switched inductor Z-source inverter," *EPE J.*, vol. 24, no. 4, pp. 14–27, Dec. 2014, doi: 10.1080/09398368.2014.11755455.

[50] N. Subhani, R. Kannan, A. Mahmud, and F. Blaabjerg, "Z-source inverter topologies with switched Z-impedance networks: A review," *IET Power Electron.*, vol. 14, no. 4, pp. 727–750, Mar. 2021, doi: 10.1049/pel2.12064.

[51] M.-K. Nguyen, Y.-C. Lim, and G.-B. Cho, "Switched-inductor quasi-Z-source inverter," *IEEE Trans. Power Electron.*, vol. 26, no. 11, pp. 3183–3191, Nov. 2011, doi: 10.1109/TPEL.2011.2141153.

[52] M. A. Ismeil, A. Abdelaleem, M. Nasrallah, and E. E. M. Mohamed, "Performance analysis of a novel high gain three-phase split source inverter," in *Proc. 23rd Int. Middle East Power Syst. Conf. (MEPCON)*, Dec. 2022, pp. 1–6, doi: 10.1109/MEPCON55441.2022.10021782.

[53] A. Abdelhakim, "Analysis and modulation of the buck-boost voltage source inverter (BBVSI) for lower voltage stresses," in *Proc. IEEE Int. Conf. Ind. Technol. (ICIT)*, Mar. 2015, pp. 926–934, doi: 10.1109/ICIT.2015.7125216.

[54] A. Abdelhakim, P. Mattavelli, V. Boscaino, and G. Lullo, "Decoupled control scheme of grid-connected split-source inverters," *IEEE Trans. Ind. Electron.*, vol. 64, no. 8, pp. 6202–6211, Aug. 2017, doi: 10.1109/TIE.2017.2677343.

[55] N. Güler, "Proportional resonant and proportional integral based control strategy for single phase split source inverters," in *Proc. 9th Int. Conf. Renew. Energy Res. Appl. (ICRERA)*, Sep. 2020, pp. 510–514, doi: 10.1109/ICRERA49962.2020.9242690.

AHMED ABDELALEEM was born in Qena Governorate, Egypt, in 1996. He received the B.Sc. degree in electrical engineering from South Valley University, Qena, Egypt, in 2019, where he is currently pursuing the master's degree with the Department of Electrical Engineering, Faculty of Engineering. He is a Teaching Assistant with the Department of Electrical Engineering, Faculty of Engineering, South Valley University. His current research interests include power electronic converters and renewable energy systems.

AHMED ISMAIL M. ALI (Member, IEEE) was born in Qena, Egypt, in 1991. He received the B.Sc. and M.Sc. degrees in electrical engineering from the Faculty of Engineering and Technology, South Valley University, Qena, in 2013 and 2017, respectively, and the Ph.D. degree in electrical engineering from Nagoya Institute of Technology, Nagoya, Japan, in 2022. Since 2013, he has been an Administrator with the Department of Electrical Engineering, Faculty of Engineering, South Valley University, where he has been a Research Assistant, since 2017. He is currently an Assistant Professor with the Department of Electrical Engineering, South Valley University. He has coauthored several publications, including PWM dc/ac inverters, bidirectional inverters, and dc/dc converters, in addition to advanced MPPT techniques for PVs and WECSs. His research interests include power electronic converters, PWM techniques, dc/ac and ac/dc converters, modular multilevel converters (MMxC), control systems, and renewable energy applications, in addition to battery chargers for electric vehicle applications. He is a Graduate Student Member of the Institute of Electrical Engineers of Japan (IEEJ). He is a member of the IEEE Power Electronics Society (PELS) and the IEEE Industry Application Society (IAS). He has been awarded the South Valley University Prize for international publishing, in 2018 and 2023.

M. NASRALLAH was born in Qena, Egypt, in 1987. He received the B.Sc. degree in electrical engineering from the High Institute of Energy, South Valley University, Egypt, in 2008, and the M.Sc. and Ph.D. degrees from the Department of Electrical Engineering, Faculty of Engineering, South Valley University, in 2013 and 2021, respectively. He is currently an Assistant Professor with the Department of Electrical Engineering, Faculty of Engineering, South Valley University. His current research interests include smart grids and renewable energy systems.

ESSAM E. M. MOHAMED (Member, IEEE) was born in Qena, Egypt, in 1974. He received the B.Sc. and M.Sc. degrees in electrical power and machines engineering from the Faculty of Energy Engineering, Aswan University, Aswan, Egypt, in 1997 and 2003, respectively, and the Ph.D. degree in electrical engineering from The University of Sheffield, Sheffield, U.K., in 2011. In 1999, he joined the Department of Electrical Engineering, Faculty of Energy Engineering, Aswan University. Since 2013, he has been with the Department of Electrical Engineering, Faculty of Engineering, South Valley University, Qena. He is currently the Founder and the Manager of the South Valley University IEEE Student Branch. His research interests include power electronics, electrical machine design and control, electric drives, and renewable energy systems.

HANY S. HUSSEIN (Senior Member, IEEE) received the B.Sc. degree in electrical engineering and the M.Sc. degree in communication and electronics from South Valley University, Egypt, in 2004 and 2009, respectively, and the Ph.D. degree in communication and electronics engineering from Egypt–Japan University of Science and Technology (E-JUST), in 2013. In 2012, he was a special Researcher Student with Kyushu University, Japan. He has been an Associate Professor with the Faculty of Engineering, Aswan University, since 2019. He is currently an Assistant Professor with the College of Engineering, King Khalid University, Saudi Arabia. His research interests include digital signal processing for communications, multimedia, image, video coding, and low-power wireless communications. He is a technical committee member of many international conferences and a reviewer of many international conferences, journals, and transactions. He was the General Co-Chair of the IEEE ITCE, in 2018.

MOHAMED A. ISMEIL was born in Qena, Egypt, in October 1977. He received the B.Sc. and M.Sc. degrees in electrical engineering from South Valley University, in 2002 and 2008, respectively, and the Ph.D. degree from the Channel System Program, Aswan University, in April 2014. From October 2010 to January 2013, he was a Ph.D. Student with the Department of Electrical Drive Systems and Power Electronics, Technical University of Munich, Germany. From April 2014 to September 2018, he was an Assistant Professor with the Faculty of Engineering, Aswan University. Since October 2018, he has been an Associate Professor with the Faculty of Engineering, South Valley University. From March 2020 to November 2022, he was the Head of the Electrical Department, Faculty of Engineering. He is currently an Associate Professor with the College of Engineering, King Khalid University, Saudi Arabia. His current research interests include power electronics applications in wind energy conversion systems, PV interface with the utility, smart grid technologies, digital control applications (PIC, FPGA, and DSP), and power inverter design for renewable applications.